Korean J. Chem. Eng., 36(7), 1102-1114 (2019)
DOI: 10.1007/s11814-018-0117-6

pISSN: 0256-1115
eISSN: 1975-7220

Iron-doped chitosan microsphere for As(III) adsorption in aqueous solution: Kinetic, isotherm and thermodynamic studies

Xiaoyu Lin, Leli Wang, Shi Jiang, Longzhe Cui, and Guiping Wu†

College of Resource and Environmental Science, South-Central University for Nationalities, Wuhan, Hubei, China
(*Received 8 Febrary 2018 • accepted 18 July 2018*)

Abstract−Iron-doped chitosan microsphere was prepared successfully and employed for effective adsorption of As(III). The results showed that the adsorption capacity benefited from the increase of iron content, and the maximum adsorption capacity was achieved at pH=8. According to the study of adsorption kinetics, adsorption rate was controlled by liquid film diffusion at a lower rotational speed, while it was controlled by chemical reaction rate at a higher rotational speed. The Freundlich and Temkin models exhibited a better fit to adsorption isotherm data, which indicated the adsorption of As(III) on iron-doped chitosan microsphere was chemisorption and the active sites of adsorbents were non-uniform distributed. Adsorption process was a spontaneous exothermic reaction because its ΔG and ΔH were negative. In presence of cations (Cd^{2+}, Pb^{2+} or Zn^{2+}) in solution, the iron-doped chitosan microsphere also showed the significant removal of As(III). However, the existence of anions (NO_3^-, SO_4^{2-} or PO_4^{3-}) inhibited the As(III) removal at different level. PO_4^{3-} showed the most significant side effects on the removal of As(III) by iron-doped chitosan microsphere. The used iron-doped chitosan adsorbent can be effectively regenerated using 1.0 mol·L^{-1} NaOH solution, and the adsorption efficiency decreased only 15.69% after being reused three times. The results of XPS, FT-IR showed that the adsorption was mainly achieved by the coordination interaction between As (III) and doped Fe in adsorbent.

Keywords: Chitosan, Adsorption, As(III), Kinetics, Isotherms

INTRODUCTION

Heavy metal pollution is usually attributed to both natural factors (rock weathering) and artificial sources, but a considerable proportion of contamination comes from human activities. Along with the over-exploitation of minerals and industrial production, excessive heavy metals are released to environment, and heavy metal pollution is becoming more and more serious [1,2]. Among these heavy metals, arsenic is one of the pervasive contaminants. In recent years, a large amount of As-containing solid residue and waste water has been yielded and discharged into environment, resulting in many serious pollution accidents, which has aroused high public concern. In the natural environment, arsenic is mostly present in inorganic forms as oxides of As(III) (H_3AsO_3, $H_2AsO_3^-$, $HAsO_3^{2-}$ and AsO_3^{3-}) and As(V) (H_3AsO_4, $H_2AsO_4^-$, $HAsO_4^{2-}$ and AsO_4^{3-}) [1,3-5]. The fact is that As(III) is more toxic than As(V) to humans, long-term drinking of arsenic-contaminated water could pose a great threat to the public health [6-10], such as "blackfoot" disease, cancer, developmental delay in children, gene mutation and so on. Due to its toxicity in human beings, in most countries, the maximum contaminant level (MCL) in potable water is set to be 50 μg·L^{-1} [11]. The World Health Organization (WHO) recommends the MCL of As in drinking water is 10 μg·L^{-1} [12,13].

In recent years, a great number of effective remediation techniques, including ion-exchange [14-16], electro-coagulation [17], membrane separation [18-20], and biological accumulation, have been studied to abate As from aqueous solution. However, each of these techniques has its own inherent limitations. Electro-coagulation treatment is ineffective at low concentrations and energy inefficient. Membrane separation requires a high cost at the early stages. Biological accumulation depends highly on environmental conditions and it is ineffective in treating high-concentration waste water. In recent years, adsorption has been considered to be an available and promising technology to conquer the above disadvantages [21], but green, nontoxic, renewable, biodegradable and highly effective adsorbents still need to be developed constantly [22]. Especially in food, drinking water and other fields, the non-toxicity of adsorbent is particularly important. Therefore, the applications of natural product-derived materials in the preparation of adsorbent have become more and more extensive. Chitosan is a non-toxic and biodegradable polysaccharide which is extracted from crabs, shrimp shell, fish scales and crab shells [21,23]. It has an overwhelming number of hydroxyl and amino groups, which are beneficial to heavy metals adsorption [21]. So chitosan has been highly regarded and listed as one of underlying low-cost adsorbents with high adsorption capacity [24]. However, its application is limited by its solubility in acidic condition. Tripoly phosphate (TPP) and glutaraldehyde ($C_5H_8O_2$) are used as crosslinker to prevent solubility of chitosan to address the limitation of application [21].

In this work, chitosan was selected as raw material to prepare adsorbent, because of its optimized properties such as easy availability, biodegradability, biocompatibility, non-toxicity [22]. Cross-

†To whom correspondence should be addressed.
E-mail: wuguiping75@hotmail.com

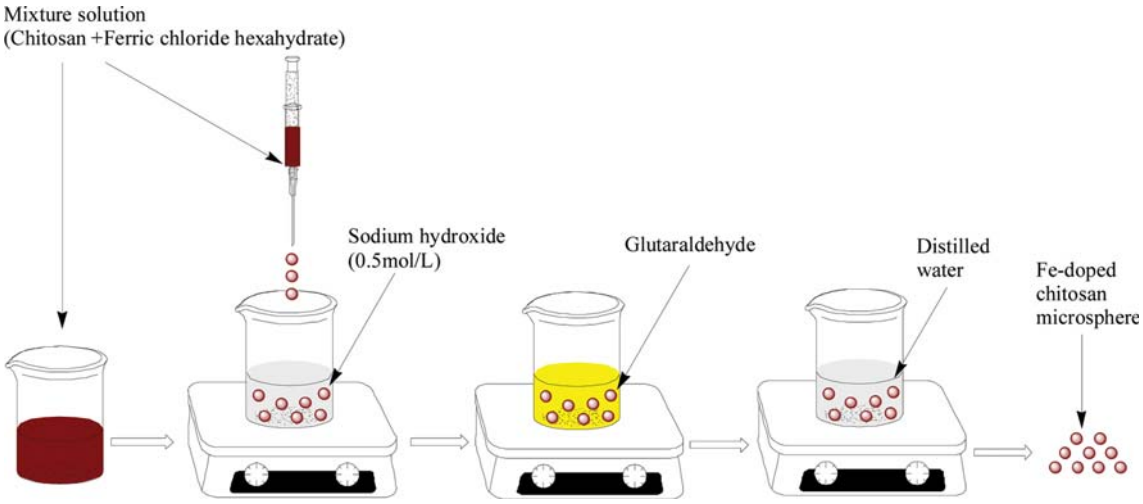

Fig. 1. Scheme of preparation process of iron-doped chitosan microsphere.

linking was used to enhance its physical properties and avoid dissolving in acidic condition. The prepared adsorbent was used to remove arsenic from water solution, and to improve its adsorption performance, iron was doped in it. Because, iron has been identified with a high affinity for arsenic and it is widely used to remove arsenic in aqueous solution. For example, nanoscale zero-valent iron, ferric oxide nanoparticles and iron oxide minerals have already been used for the arsenic removal from aqueous solution [2-4]. The powder form of iron oxides/hydroxides provides a larger specific surface area which is conducive to adsorption, but it is easy to reunite in water and dissolve in acid conditions. Meanwhile, the small particle size also drives the need for energy-intensive post-treatment filtration to recover the powder for regeneration and reuse. To overcome these limitations, embedding iron in polymer material is an effective method [25].

The prepared iron-doped chitosan microsphere can make full use of the active groups of chitosan and the affinity of iron to arsenic to get better adsorption performance. The defects of chitosan and powder iron also may be overcome through cross-linking and embedding iron in chitosan. In this study, iron-doped chitosan microsphere was used to adsorb As(III) from water in different conditions, and adsorption behavior was methodically studied with the adsorption kinetics, adsorption isotherm and adsorption thermodynamics. In addition, regeneration of iron-doped chitosan microsphere and the effect of cation and anion interference on adsorption performance were also discussed.

EXPERIMENTS

1. Materials

Chitosan (80%-95% deacetylation), acetic acid (≥99.5%), ferric chloride hexahydrate (≥99%), hydrochloric acid (36%-38%), sodium hydroxide (≥96%), sodium nitrate (≥99%), sodium sulfate anhydrous (≥99%), trisodium phosphate anhydrous (≥99%), lead(II) nitrate (≥99%), zinc nitrate hexahydrate (≥99%), cadmium nitrate (99%), glutaraldehyde (25%-28%) and sodium arsenite (≥95%) were purchased from Sinopharm Chemical Reagent Co.

2. Preparation of Chitosan Microspheres

The iron-doped chitosan microsphere was prepared as follows: (1) 6.0 g of chitosan was dissolved into 100 mL of acetic acid solution (5%) and left overnight. Certain volume of 2 $mol \cdot L^{-1}$ ferric chloride hexahydrate acetic acid solution (5%) was added into the chitosan solution, then stirred until well dissolved; (2) The mixture solution of chitosan and ferric chloride hexahydrate was added dropwise into 0.5 $mol \cdot L^{-1}$ sodium hydroxide solution by injector; (3) The resultant iron-doped chitosan microspheres were crosslinked in the glutaraldehyde solution (2.5%) about 30 min, and microspheres were washed by distilled water. The schematic of preparation process is shown in Fig. 1.

3. Batch Adsorption Experiments

3-1. Effect of Iron Content

To carry out the adsorption experiments, 0.05 g adsorbents with different iron content were weighed into triangular flasks, 50 mL solution containing 100 $mg \cdot L^{-1}$ As(III) concentration was added in, respectively. The mixture was shaken at 303.15 k for 36 h to reach equilibrium. Then, the sample was taken and filtered through 0.45 μm membrane for liquid-solid separation. The supernatant portion was used for the analysis of the residual concentration of As(III) using atomic absorption spectrometer (iCE 3500, Thermo Fisher, USA).

3-2. Effect of pH

The pH effect experiments were conducted by contacting 0.05 g adsorbent with 50 mL As(III) solution with a concentration of 100 $mg \cdot L^{-1}$ for 36 h at 303.15 K. The pH of the solution was intentionally altered by adding either HCl or NaOH aqueous solution.

3-3. Adsorption Kinetics

To study the adsorption equilibrium time and kinetic characteristics of the adsorption process, kinetic experiments were carried out by agitating 500 mL of solution containing 100 $mg \cdot L^{-1}$ As(III) concentration and 0.5 g adsorbent at 303.15 K, pH=8 at different rotational speed (50, 150, 250 $r \cdot min^{-1}$). After adsorbing for predetermined time intervals, the samples were taken and measured for As(III) concentrations. The experimental data were evaluated by four kinds of kinetic models, including pseudo-first-order, pseudo-

second-order, intra-particle diffusion model and liquid film diffusion model.

3-4. Adsorption Isotherm

The capacity of As(III) adsorbed onto iron-doped chitosan microsphere was determined by varying the initial concentration of As(III) solution within the range 10 to 500 mg·L^{-1}, which resulted in different final As(III) concentrations after adsorption equilibrium had been achieved. The experiments were conducted at 303.15 K for 24 h and pH maintained at 8. Experimental data were evaluated using Langmuir, Freundlich, BET and TemKin isotherm models to study adsorption mechanism [26,27].

3-5. Adsorption Thermodynamic

The thermodynamic analysis of As(III) adsorption by iron-doped chitosan microsphere was assessed by the energy transformation of the adsorption. 0.05 g iron-doped chitosan microsphere was added into 50 mL As(III) solution with initial concentration of 100 mg·L^{-1} at pH=8, for 36 h, at 298.15 K, 308.15 K, 318.15 K, 328.15 K and 338.15 K respectively. The experimental data were fitted by the thermodynamic models.

3-6. Coexisting Ions Influence Experiment

Coexisting ion influence experiments were performed to verify the interference of cations as well as anions commonly found in water with As(III) adsorption. The usual interference cations included Cd^{2+}, Pb^{2+} and Zn^{2+}. Mixed solution of As(III) and cations (Cd^{2+}, Pb^{2+} or Zn^{2+}) were prepared with the same concentration (50 mg·L^{-1}) of each cation. The experiments were conducted at 303.15 K and pH ranged 2 to 5. The usual interference anions included PO_4^{3-}, SO_4^{2-} and NO_3^-. Solutions containing 100 mg·L^{-1} (1.3347 mmol·L^{-1}) of As(III) were prepared containing PO_4^{3-}, SO_4^{2-} or NO_3^-. Each ion was investigated at three levels of concentration, which were 1, 1.5 and 2 mmol·L^{-1} respectively. The experiments were conducted at 303.15 K and pH=8.

3-7. Regeneration of Iron-doped Chitosan Microsphere

To regenerate iron-doped chitosan microsphere, the spent adsorbent was soaked in NaOH solution with concentration of 0.1 mol·L^{-1}, 0.5 mol·L^{-1} or 1.0 mol·L^{-1} and stirred at 298.15 K for 16 h. Then the adsorbent was washed with deionized water and used to adsorb As(III) again. The above procedure was carried out for three cycles of repeated adsorption/desorption to determine reusability efficacy of the iron-doped chitosan microsphere.

3-8. Characterization

FTIR (Spectrum GX, PERKIN-Elmer, USA) instrument was used for measurement the functional groups existing in iron-doped chitosan microsphere within the range of 400-4,000 cm^{-1}; the samples were prepared as KBr disks. Atomic valence states of O, N, Fe and As were measured by X-ray photoelectron spectroscopy (XPS) (Thermo Electron Corporation, MULTILAB2000, USA) instrument with monochromatic Al Ka as the X-ray source (1486.71 eV of photons).

RESULTS AND DISCUSSION

1. Effect of Iron Content in Adsorbent

The results of the effect of iron content in adsorbent on the As(III) adsorption are shown in Fig. 2. The chitosan microsphere without iron doping showed a poor adsorption performance for As(III), and the adsorption capacity increased from 3 to 70 mg·g^{-1} with the increase of iron content from 0 to 6.79%. The results showed that iron doping in adsorbent played important roles in the adsorption process. Because As(III) exists in the form of H_2AsO^-, $HAsO_3^{2-}$ and AsO_3^{3-} in solution. H_2AsO^-, $HAsO_3^{2-}$ and AsO_3^{3-} can combinate with Fe through sharing lone pair of electrons and vacant orbital. So iron-doped chitosan microsphere could adsorb As(III) by forming Fe-O-As coordination bonds [28-30]. Accordingly, the adsorption capacity of As(III) increases with the increase of iron content. However, it was failed to prepare iron-dope chitosan microsphere which iron content was higher than 6.79%, because chitosan and ferric chloride hexahydrate cannot form a fully dissolved mixed solution when Fe doping is higher than 6.79%. Thus, chitosan microsphere with iron content of 6.79% was selected to use in the following adsorption study.

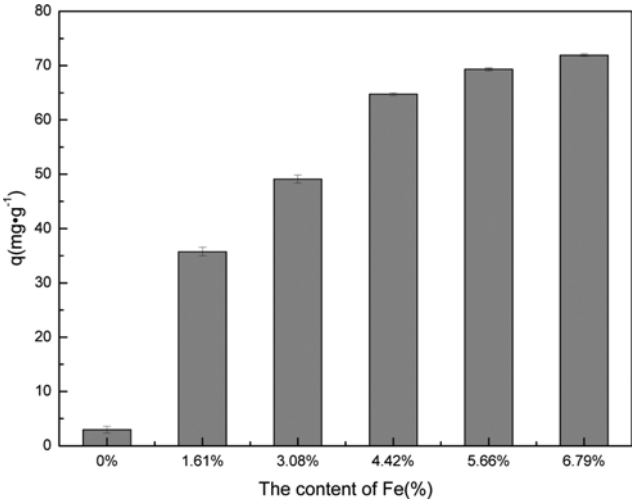

Fig. 2. Effects of Fe content on the As(III) adsorption.

2. Effect of pH on As(III) Adsorption

pH plays a significant role in adsorption-based water treatment processes, because of the speciation of As(III), the surface charge and the stability of adsorbent are strongly influenced by the water pH value. The adsorption capacity of As(III) on iron-doped chitosan microsphere, the Fe concentration in solution after adsorption equilibrium had been achieved and the forms of As(III) at different pH are shown in Fig. 3(a)-(c). As shown in Fig. 3(a), as the pH was increased, the adsorption capacity of As(III) increased and the maximum adsorption capacity was obtained at pH=8. However, when pH>8 the uptake declined with the increasing of pH.

Fe doped in adsorbent may be dissolved out, especially under acidic conditions. As shown in Fig. 3(b), when pH≥5, the concentration of Fe in the solution is negligible. The result shows that iron-doped chitosan microsphere is stable under the condition of pH≥5. But the adsorbent stability is poor in solution with pH less than 5. Moreover, the more acidic the solution, the worse the stability of adsorbent. The instability of adsorbent may be one of the reasons for the lower adsorption capacity under acidic conditions. Meanwhile, the amino group of chitosan was protonated to being $-NH_3^+$ under acidic conditions, which impeded the adsorption of positive ions such as $As(OH)^{2+}$, and it was not helpful to the adsorp-

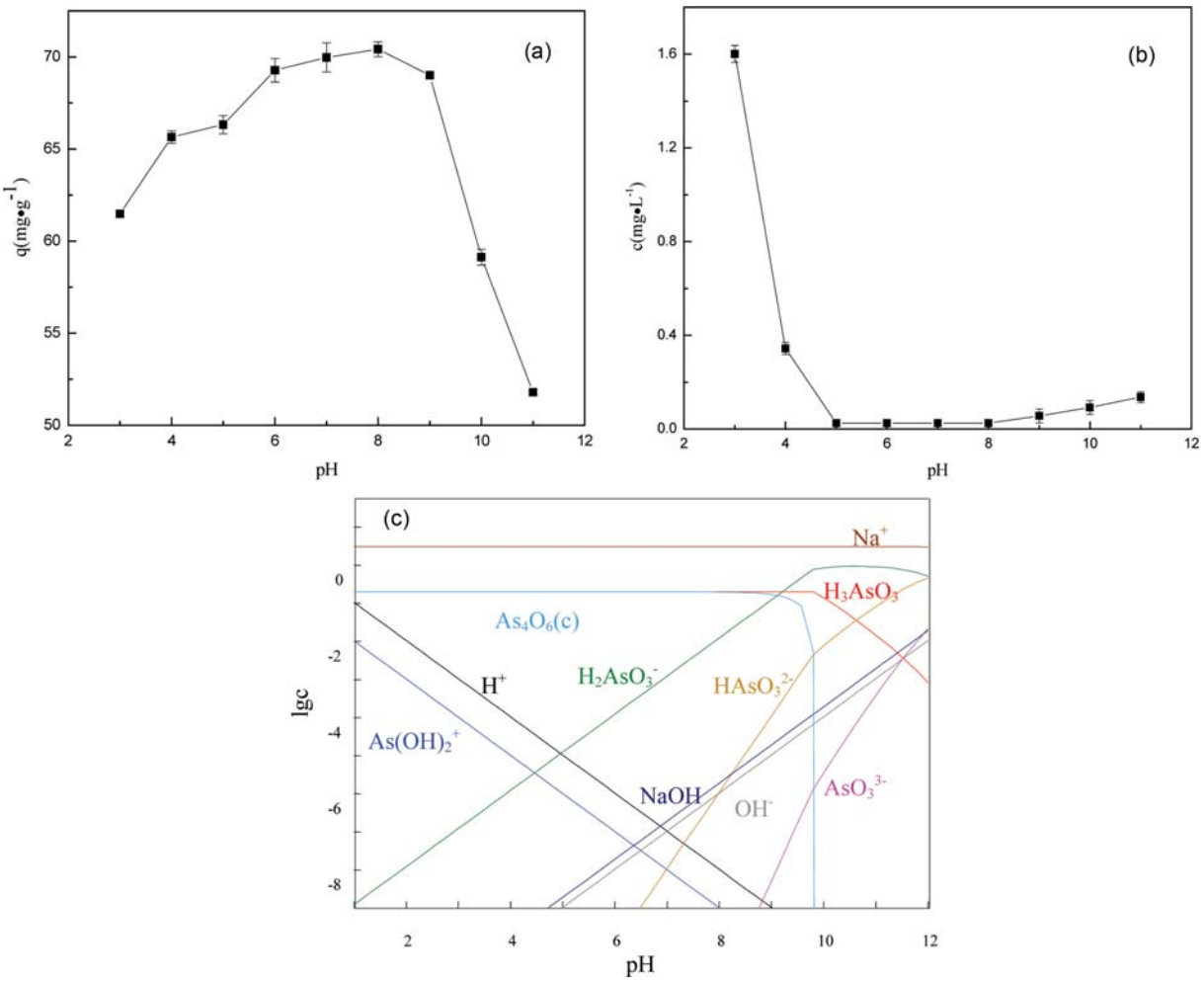

Fig. 3. (a) Effects of pH on the As(III) on Fe-doped chitosan microsphere, (b) Concentrations the dissolved iron at different pH, (c) Forms of As(III) at different pH ($c_{As(III)}$=100 mg·L^{-1}, T=298.15 K).

tion of neutral components such as H_3AsO_3 and As_4O_6. As the pH of the solution increased, the stability of the adsorbent was enhanced and the degree of amino-protonation decreased, the concentration of positive $AS(OH)^{2+}$ decreased while the concentrations of negative $H_2AsO_3^-$ and $HAsO_3^{2-}$ increase; these all are beneficial to As(III) reaching to the surface of iron-doped chitosan microsphere through electrostatic interaction [31]. So the adsorption capacity of As(III) adsorption on iron-doped chitosan microsphere increased with the increase of pH. However, with pH>8, the result was contrary to the former, which was attributed to the presence of excess OH^-, and OH^- would compete with negative $H_2AsO_3^-$, $HAsO_3^{2-}$ and AsO_3^{3-} for the adsorption sites on the surface of the adsorbent [32-34]. Meanwhile, the stripping amount of iron increased with the increasing of pH value at pH>8. This also has an adverse impact for As(III) adsorption on iron-doped chitosan microsphere. The maximum adsorption capacity was achieved at pH=8. Thus, pH=8 was selected to use in the entire study.

3. Adsorption Kinetics

Adsorption kinetics curves are shown in Fig. 4. The As(III) adsorption on iron-doped chitosan microsphere was rapid at initial phase. There might have been an overwhelming number of active sites for adsorption at the initial phase. Subsequently, the rate of adsorption decreased relatively with the extension of contact time

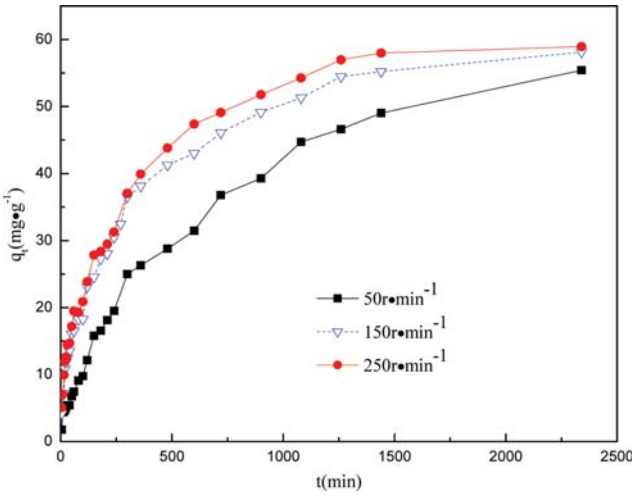

Fig. 4. Effect of contact time on adsorption of As(III).

until adsorption equilibrium. And the increase of rotational speed was beneficial to the rate of adsorption process. The possible reason might be that the presence of liquid film in the solid-liquid contact interface inhibits the diffusion of As(III) to adsorbent surface, and increasing of the rotational speed would reduce the thickness of the liquid film, thus increasing the adsorption rate.

According to the present state of knowledge, adsorption of a species on a solid surface follows four steps: (i) transport of the adsorbate (ions in case of solutions) from the bulk to the external surface of the adsorbent; (ii) diffusion of solute across the liquid film surrounding sorbent particles (liquid film diffusion); (iii) diffusion of solute in the liquid contained in the pores of sorbate particle and along the pore walls (intraparticle diffusion); and (iv) interactions with the surface atoms of the solid leading to chemisorption (strong adsorbate-adsorbent interactions equivalent to covalent bond formation) or weak adsorption (weak adsorbate-adsorbent interactions, very similar to van der Waals forces) and desorption of solute molecules on/from the sorbent surface [35]. The overall sorption rate may mainly be controlled by any of these steps; a combined effect of a few steps is also possible [36-38]. To study the kinetic characteristics of the adsorption process, the pseudo-first-order, pseudo-second-order, intra-particle diffusion model and liquid film diffusion model were applied for the adsorption of As(III) ions on iron-doped chitosan microsphere.

Pseudo-first-order is based on membrane diffusion theory, which holds that the adsorption rate is proportional to the first power of the difference between equilibrium adsorption capacity and adsorption capacity. The adsorption process is governed by the diffusion step (membrane diffusion or intra-particle diffusion) [39]. The pseudo-first order equation is shown in Eq. (1),

$$\lg(q_e - q_t) = \lg q_e - \frac{k_1}{2.303}t \quad (1)$$

where q_e is the adsorption capacity at equilibrium ($mg \cdot g^{-1}$), q_t is the adsorption amounts at time t ($mg \cdot g^{-1}$), k_1 is the pseudo-first-order rate constant.

Pseudo-second-order kinetics is based on the assumption that the adsorption rate is controlled by the chemical adsorption rate,

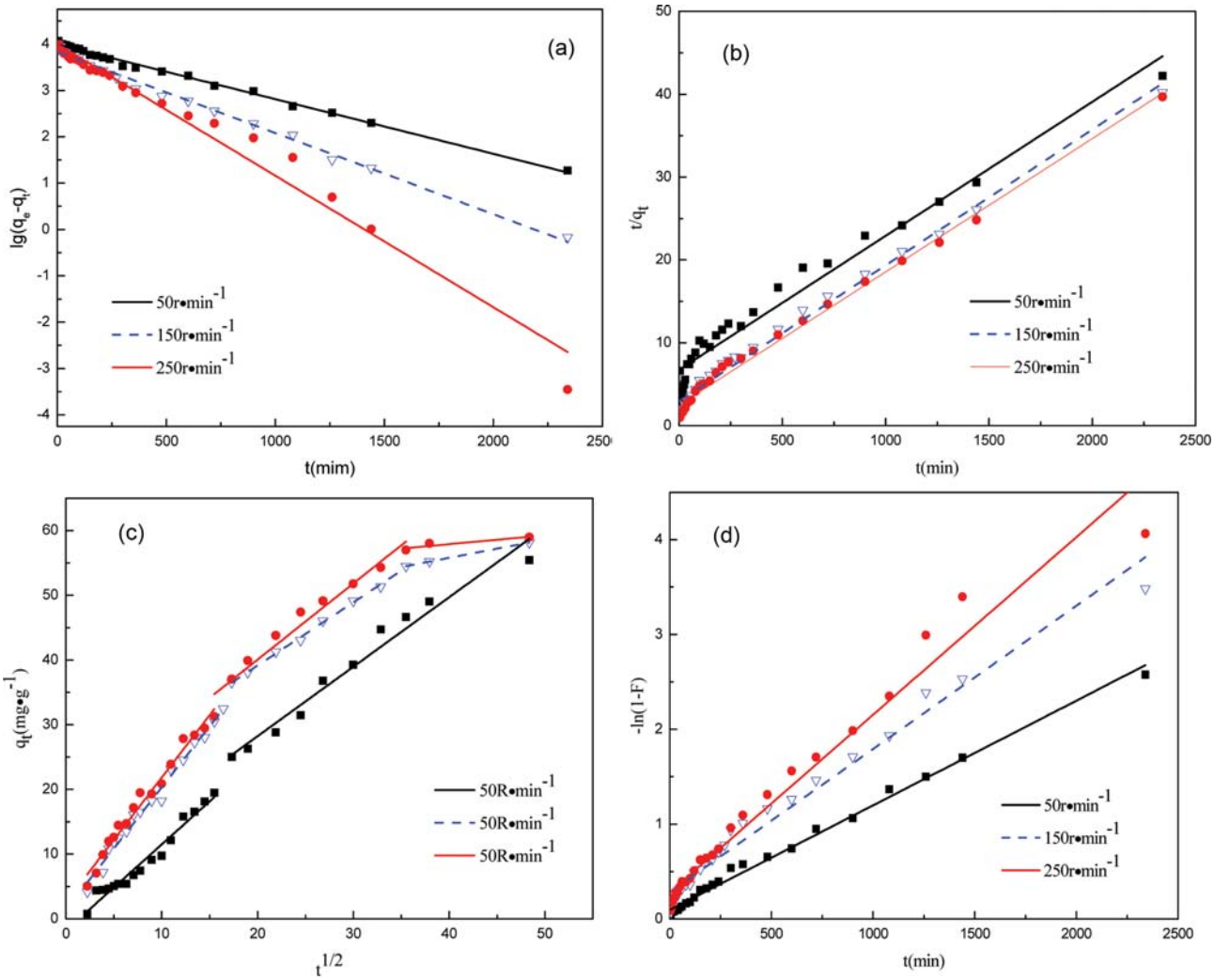

Fig. 5. Adsorption kinetics of As(III) adsorption by Fe-doped chitosan microsphere, (a) pseudo-first-order, (b) pseudo-second-order, (c) intra-particle diffusion model and (d) liquid film diffusion model.

which adsorption involves the sharing or transfer of electron pairs between the adsorbent and the adsorbate [39,40]. The pseudo-second-order equation is shown in Eq. (2),

$$\frac{t}{q_t} = \frac{1}{k_2 q_e^2} + \frac{t}{q_e} \quad (2)$$

where q_e is the adsorption capacity at equilibrium ($mg \cdot g^{-1}$), q_t is the adsorption amounts at time t ($mg \cdot g^{-1}$), k_2 is the pseudo-second-order rate constant.

Intra-particle diffusion model equation can be expressed as Eq. (3). If the line of q_e vs. $t^{1/2}$ has zero intercept (C_i=0) the adsorption process was controlled by intra-particle diffusion [37,41-43].

$$q_e = k_i \times t^{1/2} + C_i \quad (3)$$

where q_e is the adsorption capacity at equilibrium ($mg \cdot g^{-1}$), k_i is the intra-particle diffusion rate constant and, C_i is the thickness of the boundary layer.

Liquid film diffusion model is expressed as follows Eq. (4), the line of $-\ln(1-F)$ vs. t passed through the origin (C_l=0), indicating that the adsorption process was controlled by liquid film diffusion [44].

$$-\ln(1-F) = k_l t + C_l \quad (4)$$

where k_l is Liquid film diffusion model rate constant, F can be calculated by dividing q_t by q_e.

The results of pseudo-first-order and pseudo-second-order are represented in Fig. 5(a) and Fig. 5(b), respectively. The values of parameters are summarized in Table 1. In contrast to the value of R^2, it was concluded that the adsorption process was more fit to the pseudo-first-order under rotational speed 50 and 150 $r \cdot min^{-1}$, which indicated the adsorption process was controlled by the diffusion step (membrane diffusion or intra-particle diffusion) [39]. Conversely, the experimental data were more suitable to pseudo-second-order at 250 $r \cdot min^{-1}$, which implies that the adsorption process involves the formation of valency forces through the exchange or sharing of electrons between AS(III) ions and the binding sites of iron-doped chitosan microsphere. The result suggested that the adsorption process was governed by the chemical adsorption rate under rotational speed 250 $r \cdot min^{-1}$ [39,40,45]. It can also be seen that the rotational speed has a great influence on the rate constants (k_1 and k_2). K_1 and k_2 increased as rotational speed increased. It can be explained that As(III) ions move more active at the higher rotational speed. The higher collision frequency of As(III) ions and adsorbent surface and the thinner liquid film lead a greater adsorption rate [40]. The calculation results are in conformity with the experimental results.

The result of intra-particle diffusion model is graphically shown in Fig. 5(c), and values of parameters are listed in Table 2. As shown in Fig. 5(c), the adsorption process was divided into three stages at high rotational speed (150 $r \cdot min^{-1}$, 250 $r \cdot min^{-1}$). The first stage was owing to liquid film diffusion and external surface adsorption stage. The second stage was gradual adsorption stage attributable to intraparticle diffusion. The last stage was the final equilibrium stage [46]. The adsorption process was divided into two stages at 50 $r \cdot min^{-1}$, the final equilibrium stage had not been achieved due to slow adsorption rate. The results in Fig. 5(c) and Table 2 showed that the adsorption of As(III) ions on iron-doped chitosan microsphere was not merely controlled by the intra-particle diffusion. In addition to intra-particle diffusion, there were some other factors such as liquid film diffusion and chemisorption also involved in controlling the adsorption process. $K_{p1(250\ r \cdot min^{-1})} > K_{p1(150\ r \cdot min^{-1})} > K_{p1(50\ r \cdot min^{-1})}$, which suggested that thickness of liquid film was decreased with increasing the rotational speed. It became easier for a multitude of As(III) ions diffusion through the liquid film and interacting with active sites on adsorbent (high adsorption intensity), which was favorable for the increase of adsorption rate. As shown in Fig. 5(c) and Table 2, the intercept (C_i) was increased with increasing time and exhibited the increasing in the boundary layer diffusion effect, due to the As(III) ions entering into the pores of adsorbent. Accordingly, the adsorption mechanism of As(III) ions on the surface of iron-doped chitosan microsphere was convoluted because of both the intra particle diffusion and surface diffusion contributes to the adsorption process [34]. In addition to the diffusion rate constants of same rotational speed following the order of $K_{p1} > K_{p2} > K_{p3}$ (Fig. 5(c) and Table 2), the rate constant (K_{p1}) for adsorption of As(III) ions on iron-doped chitosan microsphere was prominently higher than others (K_{p2} and K_{p3}), which might be attributed to the existence of fresh active sites on iron-doped chitosan microsphere surface [34].

The liquid film diffusion model and parameter values are shown in Fig. 5(d) and Table 1, respectively. The intercept (C_l) was approxi-

Table 1. The parameters of the As(III) adsorption for the pseudo-first-order, pseudo-second-order and liquid film diffusion model

Rotational speed ($r \cdot min^{-1}$)	Pseudo-first-order		Pseudo-second-order		Liquid film diffusion model			
	R^2	K_1 (min^{-1})	R^2	K_2 ($g \cdot mg^{-1} \cdot min^{-1}$)	R^2	K (min^{-1})	$t_{1/2}$ (min)	c
50	0.9957	0.0042	0.9600	0.00004	0.9931	0.0011	544.27	0.0945
150	0.9914	0.0041	0.9860	0.00009	0.9764	0.0015	271.55	0.2831
250	0.9739	0.0065	0.9926	0.00011	0.9693	0.0019	227.77	0.2809

Table 2. The parameters of the As(III) adsorption for the intra-particle diffusion model

Rotational speed (r/min)	R_1^2	K_{p1}	C_1	R_2^2	K_{p2}	C_2	R_3^2	K_{p3}	C_3
50	0.9643	1.332	−1.821	0.9652	1.074	6.737	-	-	-
150	0.9850	1.891	1.405	0.9974	0.977	19.61	0.9996	0.2839	44.28
250	0.9788	1.967	2.570	0.9533	1.178	16.49	0.7638	0.1357	52.48

mately equal to zero at 50 r·min^{-1}. It showed that liquid film diffusion was the main controlling factor of the adsorption process. The liquid film outside iron-doped chitosan microsphere surface was thicker at slow rotational speed (50 r·min^{-1}). It was difficult for As(III) ions to get through the liquid film. Therefore, the adsorption process was controlled by liquid film diffusion. This implied that the rate of liquid film diffusion was the slowest in whole adsorption process at 50 r·min^{-1}. The $t_{1/2(50\ r\cdot min^{-1})}>t_{1/2(150\ r\cdot min^{-1})}>t_{1/2(250\ r\cdot min^{-1})}$, which shows that the increase of rotational speed was beneficial to the rate of the adsorption process. The $t_{1/2(250\ r\cdot min^{-1})}$ of the adsorption of As(III) was 277.77 min, which means that the adsorption velocity of As(III) on iron-doped chitosan microsphere under 250 r·min^{-1} was considerably slow. The result implied that the use of iron-doped chitosan microsphere was limited in the application of packed columns for continuous adsorption except as the length of the packed column was long enough, otherwise the velocity of wastewater was slow enough.

4. Adsorption Isotherm

The adsorption isotherm experiments were carried out at different initial concentrations. The result is shown in Fig. 6. The adsorption capacity of As(III) sharply increased with the increasing As(III) equilibrium concentration from 0 to 90 mg·g^{-1}. It would be that there were abundant extra active sites that were not be occupied when the equilibrium concentration of As(III) was less than 90 mg·L^{-1}. However, adsorption capacity did not enhance greatly with the increase of As(III) concentration when equilibrium concentration of As(III) ions was higher than 90 mg·L^{-1}. Experimental data were evaluated using different isotherm models: Langmuir, Freundlich, BET and Temkin.

Langmuir model was identified as valid for monolayer adsorption, which assumed that the surface of adsorbent was homogeneous and there was no interaction among the adsorbent molecules [45-47]. This model could be linearized by an equation as Eq. (5) [48]. R_L (separation factor or equilibrium parameter) as an important parameter that defines the main characteristics of Langmuir model shows the state and condition of isotherm model. If R_L=0, 0<R_L<1, R_L=1 and R_L>1, then the process is defined to be irreversible, desirable, linear and undesirable, respectively [41,48,49]. The value of R_L was calculated using Eq. (6)

$$\frac{c_e}{q_e}=\frac{c_e}{q_m}+\frac{1}{k_L q_m} \tag{5}$$

$$R_L=\frac{1}{1+K_L c_0} \tag{6}$$

The Freundlich isotherm describes the relationship between non-ideal and reversible adsorption. This model is applied to adsorption on heterogeneous surfaces with the interaction between adsorbed molecules. The application of the Freundlich equation also suggests that sorption energy exponentially decreases upon the completion of the sorption centers of the adsorbent. Adsorption in Freundlich model was not limited by the monolayer adsorption [46,50]. The data of equilibrium was studied following the Freundlich model equation as Eq. (7). The value of 1/n was less than 1; it indicates that the adsorption process was easy to implement [51]. Oppositely, it indicates that the adsorption process was more difficult to realize when 1/n was greater than 2 [34].

$$\ln q_e=\ln k_F+\frac{1}{n}\ln c_e \tag{7}$$

The BET isotherm is widely used to describe multilayer sorption phenomena. BET assumes that adsorbent surfaces are perfectly flat and that molecules can be adsorbed on this surface or pile on top of another molecule that is already adsorbed [52]. Van der Waals force played a major role between adsorbent and adsorbate. The adsorption would be considered to be dominated by physical adsorption if the experimental data fitted the BET model. The BET equation linearizes the curved part of the isotherm that occurs near the monolayer completion (Eq. (8)) [53,54].

$$\frac{c_e}{q_e(c_0-c_e)}=\frac{B-1}{q_e^n B}\times\frac{c_e}{c_0}+\frac{1}{q_e^n B} \tag{8}$$

The Temkin isotherm takes into account that the presence of indirect adsorbate/adsorbate interactions affects the heat of adsorption of all adsorbed molecules in the layer would decrease linearly with coverage [27,45]. A straight line q_e *vs.* ln(C_e) could be obtained by Temkin model as shown as Eq. (9). The adsorption process was considered as chemical process if the experimental data fit the Temkin model.

$$q_e=B_T\times(\ln A+\ln c_e) \tag{9}$$

where q_e is the adsorption amount at equilibrium (mg·g^{-1}), q_m is the maximum adsorption capacity (mg·g^{-1}). C_0 and C_t are the concentration of As(III) in solution (mg·L^{-1}) at initial and equilibrium concentration, respectively. k_L (L·mg^{-1}) and k_F (g·mg^{-1}) are Langmuir and Freundlich equilibrium adsorption constants, respectively. 1/n is the empirical parameter, B is the maximum adsorption capacity of the monolayer adsorption (mg·g^{-1}), A is an equilibrium binding constant, B_T is an isotherm constant of Temkin model.

The fitting results of Langmuir and Freundlich model are shown in Fig. 7(a) and (b), respectively. Values of parameters are shown in Table 3. The adsorption of As(III) onto iron-doped chitosan microsphere showed a better linearity with Freundlich model, which

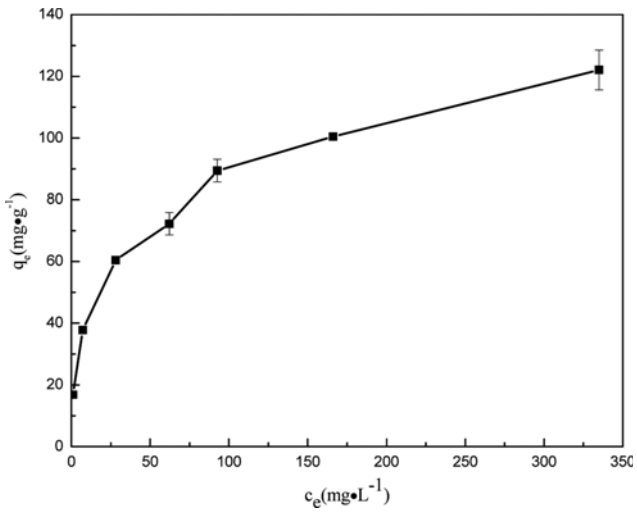

Fig. 6. Effect of concentration on adsorption of As(III).

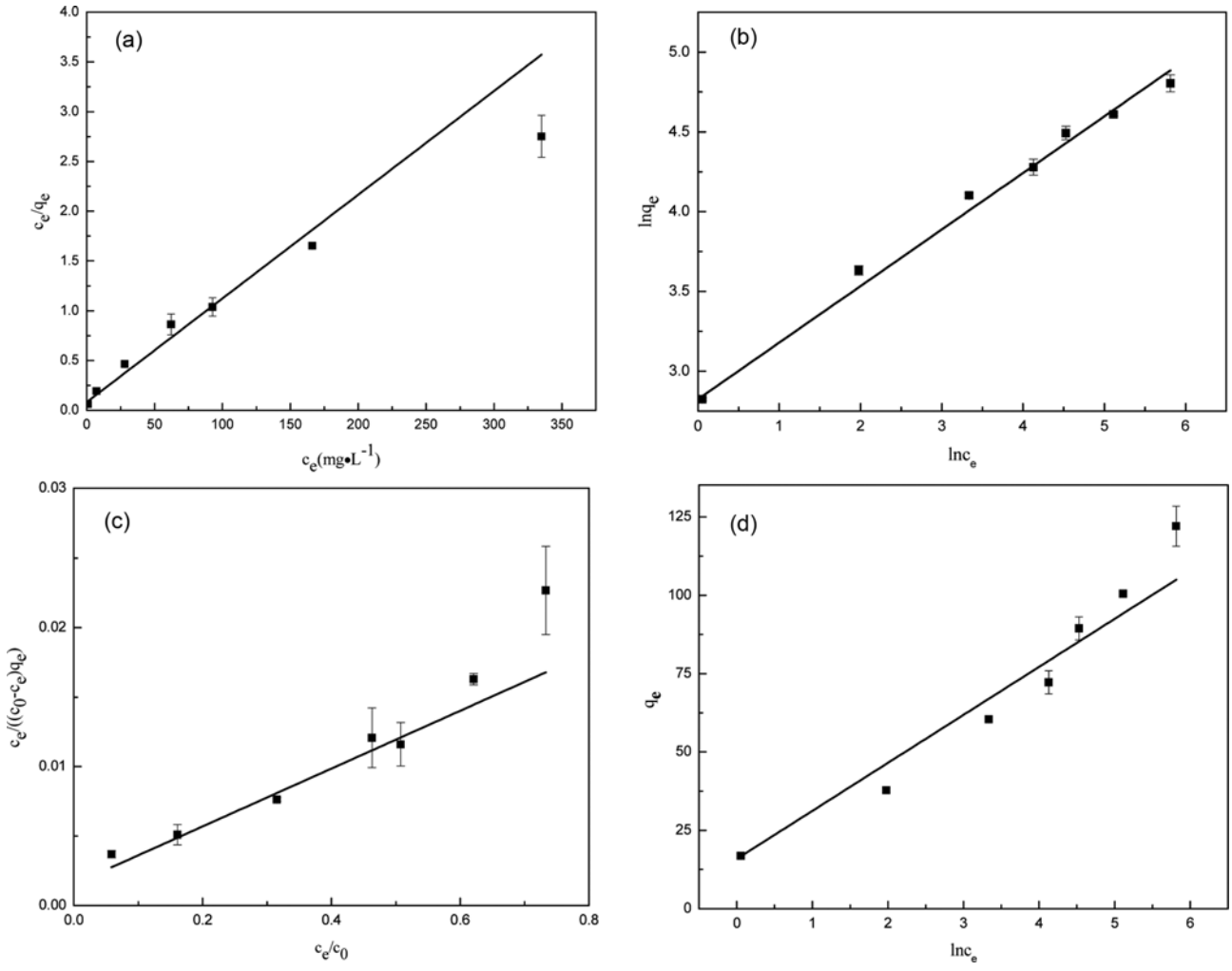

Fig. 7. Adsorption isotherm of As(III) adsorption onto iron-doped chitosan microsphere, (a) Langmuir, (b) Freundlich, (c) BET and (d) TemKin model.

Table 3. The parameters of the As(III) adsorption for adsorption isotherm models

Model	Langmuir				Freundlich			BET			Temkin		
Parameter	R^2	K_L	q_m	R_L	R^2	K_F	1/n	R^2	q_e^n	B	R^2	B_T	A
Value	0.947	0.127	95.97	0.02-0.30	0.996	16.85	0.355	0.918	44.77	14.60	0.982	15.88	2.818

indicated adsorption was not limited by the monolayer adsorption and adsorbent interacted with adsorbate by non-uniform surface [46]. Moreover, the value of 1/n (0.3546) was less than 1, which indicated the adsorption could occur in normal condition [51].

The fitted lines of BET and TemKin isotherm model are shown in Fig. 7(c) and (d), respectively. Parameters are listed in Table 3. Compared to the BET model, the R^2 of Temkin isotherm model was closer to 1. The result shows that heat of adsorption decreases linearly with the increase of degree of coverage. Thus, chemisorption dominated in the adsorption of As(III) on iron-doped chitosan microsphere.

Although it was difficult to compare the iron-doped chitosan microsphere directly with other adsorbents because of different applied experimental conditions, the adsorption capacity for As(III) on the granular iron-doped chitosan microsphere was reasonably higher compared with other granular adsorbents (Table 4). These results demonstrated that the iron-doped chitosan microsphere showed good adsorption performance for As(III).

5. Adsorption Thermodynamic

Temperature played a significant role in the adsorption process. The effect of temperature on the adsorption of As(III) on iron-doped chitosan microsphere is given in Fig. 8. As shown, low temperature was conductive to the adsorption and the adsorption capacity of As(III) decreased with the temperature increasing.

The Gibbs free energy (ΔG) was calculated by Eq. (10) [60]. Enthalpy change (ΔH) and entropy change (ΔS) could be determined from the equation with Eq. (11) and Fig. 9 [31,61]. Values of thermodynamic parameters are given in Table 5. ΔG of less than 0

Table 4. Comparison of adsorption capacity with different adsorbents

Adsorbent	q_m (mg·g^{-1})	Reference
Novel chitosan goethite bionanocomposite beads	8.47	[25]
Fe-sericite composite beads	9.02	[55]
Fe-sericite composite powder	15.04	[55]
Calcined Cardita bicolor	60.98	[48]
Novel hydrous iron-nickel-manganese	81.9	[49]
Novel mixed Ce-Fe oxide decorated multiwalled	28.74	[56]
Calix[4]pyrrole	14.29	[1]
Ultrafine α-Fe_2O_3 nanoparticles	95	[3]
Fe-based backwashing sludge	59.7	[35]
Fe-Mn binary oxide impregnated chitosan bead	54.2	[57]
Novel Fe-Mn modified biochar composite	8.25	[58]
Flowerlike Fe_3O_4	9.03	[59]
Iron-doped chitosan microsphere	≥125	This study

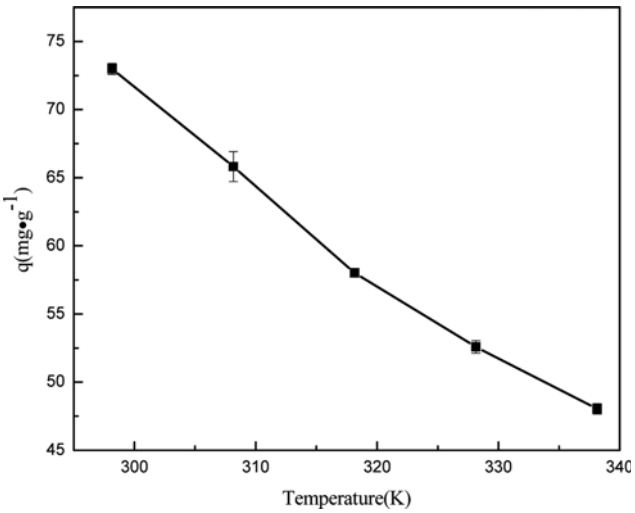

Fig. 8. Effect temperature of on adsorption of As(III).

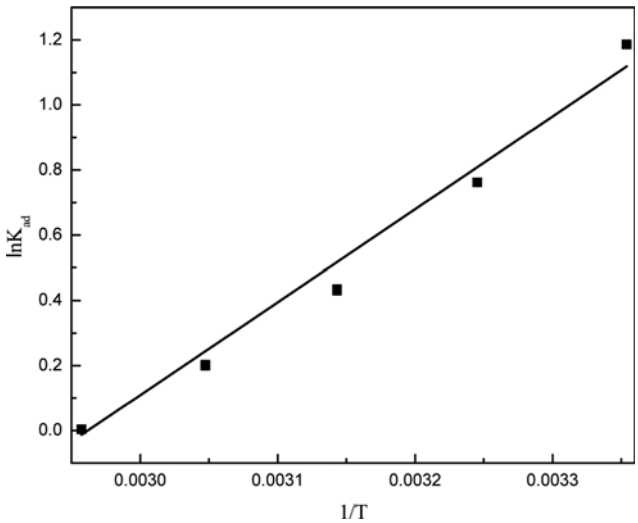

Fig. 9. Adsorption thermodynamic of As(III) adsorption.

indicated that the adsorption of the As(III) on iron-doped chitosan microsphere was spontaneous. The negative value of ΔH (−23.71 kJ·mol^{-1}) indicated that the adsorption process of As(III) on iron-doped chitosan microsphere was exothermic. Which could be explained that new chemical bonds or coordination bonds (Fe-O-As) were formed during the adsorption process. The equilibrium of adsorption was shifted toward desorption with the temperature rising [42]. Thus, iron-doped chitosan microsphere could be well used to remove As(III)-containing wastewater at room temperature. ΔS and ΔH were less than 0, which suggested that the spontaneous adsorption of As(III) onto iron-doped chitosan microsphere was driven by reducing system energy. Spontaneous reactions have two main drivers: The energy of the reaction system decreases (ΔH< 0) and the chaos of the system increases (ΔS>0). As shown in Table 5, ΔS and ΔH were less than 0, indicating the spontaneous process of iron-doped chitosan microsphere for As(III) adsorption was driven by the energy of the reaction system decreases.

$$\Delta G = -RT\ln K_{ad} \tag{10}$$

Table 5. The parameters of the As(III) adsorption for adsorption thermodynamic

T (K)	ΔG (kJ·mol^{-1})	ΔH (kJ·mol^{-1})	ΔS (J·mol^{-1}·K^{-1})
298.15	−2.94		
308.15	−1.95		
318.15	−1.14	−23.71	−70.22
328.15	−0.55		
338.15	−0.01		

$$\ln K_{ad} = \frac{\Delta S}{R} - \frac{\Delta H}{R} \times \frac{1}{T} \tag{11}$$

where T is the temperature of the adsorption system (K), R is the gas constant 8.314 J·mol^{-1}·K^{-1}, and k_{ad} is the adsorption coefficient.

6. Interference of Coexisting Ions

Fig. 10(a) illustrates the influences of coexisting positive Pb^{2+}, Zn^{2+} and Cd^{2+} ions on the removal of As(III) by iron-doped chitosan microsphere. It can be seen that the coexisting of Pb^{2+}, Zn^{2+}

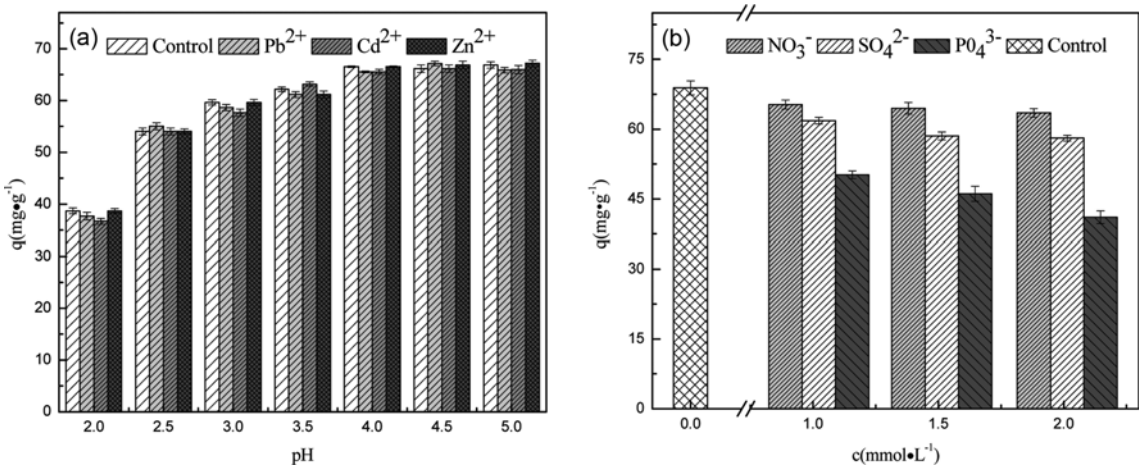

Fig. 10. Influences of interference ions on the adsorption of As(III) by iron-doped chitosan microsphere. (a) Cation, (b) anion.

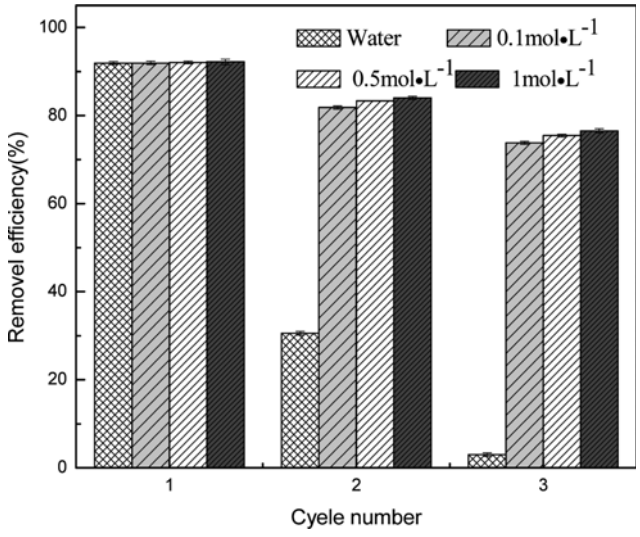

Fig. 11. Recyclability tests in As(III) adsorption on iron-doped chitosan microsphere.

and Cd^{2+} ions in solution had a negligible influence on the adsorption capacity of As(III). The reason might be Fe in iron-doped chitosan microsphere plays a significant role in adsorption of As(III). However, Fe was unable to bind Pb^{2+}, Zn^{2+} and Cd^{2+} ions, so active sites for the adsorption of As(III) in iron-doped chitosan microsphere could not be occupied by Pb^{2+}, Zn^{2+} and Cd^{2+} ions.

Fig. 10(b) shows the influences of the coexisting anionic on the binding of As(III) to the iron-doped chitosan microsphere. As shown in Fig. 11, the existence of NO_3^-, SO_4^{2-} and PO_4^{3-} inhibited the As(III) removal at different level. The experiment results show that for As(III) adsorption, the competing anions effect were basically in the order of $PO_4^{3-}>SO_4^{2-}>NO_3^-$. PO_4^{3-} showed the most significant side effect on the removal of As(III) by iron-doped chitosan microsphere. With the concentrations of PO_4^{3-} increasing from 0 to 1, 1.5 and 2 $mmol\cdot L^{-1}$, the adsorption capacity of As(III) was obviously decreased from 68.75 to 51.09, 46.17 and 40.13 $mg\cdot g^{-1}$. Many reports were identified that were not occupied can efficiently reduce the adsorption of As(III) due to the competition for adsorption sites [32,62,63]. Fe in iron-doped chitosan microsphere could be occupied by PO_4^{3-} through forming Fe-O-P coordination bonds [62].

7. Regeneration of Iron-doped Chitosan Microsphere

The stability and regeneration quality of the sorbent are of great significance in practical application. Fig. 11 shows the removal efficiency for As(III) using fresh and recycled adsorbent which has been regenerated using NaOH solution with different concentrations. The results show that iron-doped chitosan microsphere retained considerable adsorption efficiency in spite of the loss of adsorption capacity during every recycle, and the concentration of NaOH solution has no obvious influence on the regeneration efficiency. The removal efficiency of As(III) was still up to 76.52% with iron-doped chitosan microsphere which regenerated twice by 1.0 $mol\cdot L^{-1}$ NaOH as adsorbent, only reduced nearly 15.69% comparison with the fresh adsorbent. This revealed that iron-doped chitosan microsphere can be efficiently regenerated by NaOH solution as a kind of promising adsorbent for As(III). When As(III)-adsorbed iron-doped chitosan microsphere was immersed NaOH solution, As(III) ions could desorb from iron-doped chitosan microsphere through hydroxyl exchange [49].

8. Characterization and Sorption Mechanism

To further probe into the mechanism of adsorption As(III) by iron-doped chitosan microsphere, XPS was used to characterize the C ls, O 1s, N 1s, Fe 2p and As 3d (before and after sorption). The scans for O 1s, N 1s, Fe 2p and As 3d are shown in Fig. 12(a)-(d), respectively.

As shown in Fig. 12(a), the O 1s spectra was mainly divided into six peaks corresponding to Fe-O (529.5 and 530.5 eV), O-H (531.5 eV), C-O (532.4 eV), C=O (533.1 eV) and C-O-C (533.7 eV) [28, 64-66]. After adsorption, the component of peak area of Fe-O at 530.5 eV was greatly increased (from 15.93% to 23.18%), which was assigned to As(III) ($AS(OH)^{2+}$, H_3AsO_3, H_2AsO^-, $HAsO_3^{2-}$ or AsO_3^{3-}) adsorption onto Fe-doped chitosan microsphere through forming Fe-O-As coordination bonds [28]. This allowed component of peak area of Fe-O increase. The peaks of N1s spectrum regarding Fe-doped chitosan microsphere are revealed in Fig. 12(b). There are three peaks at 399.9 eV, 399.4 eV and 398.9 eV in the N 1s XPS spectrum of iron-doped chitosan microsphere, which rep-

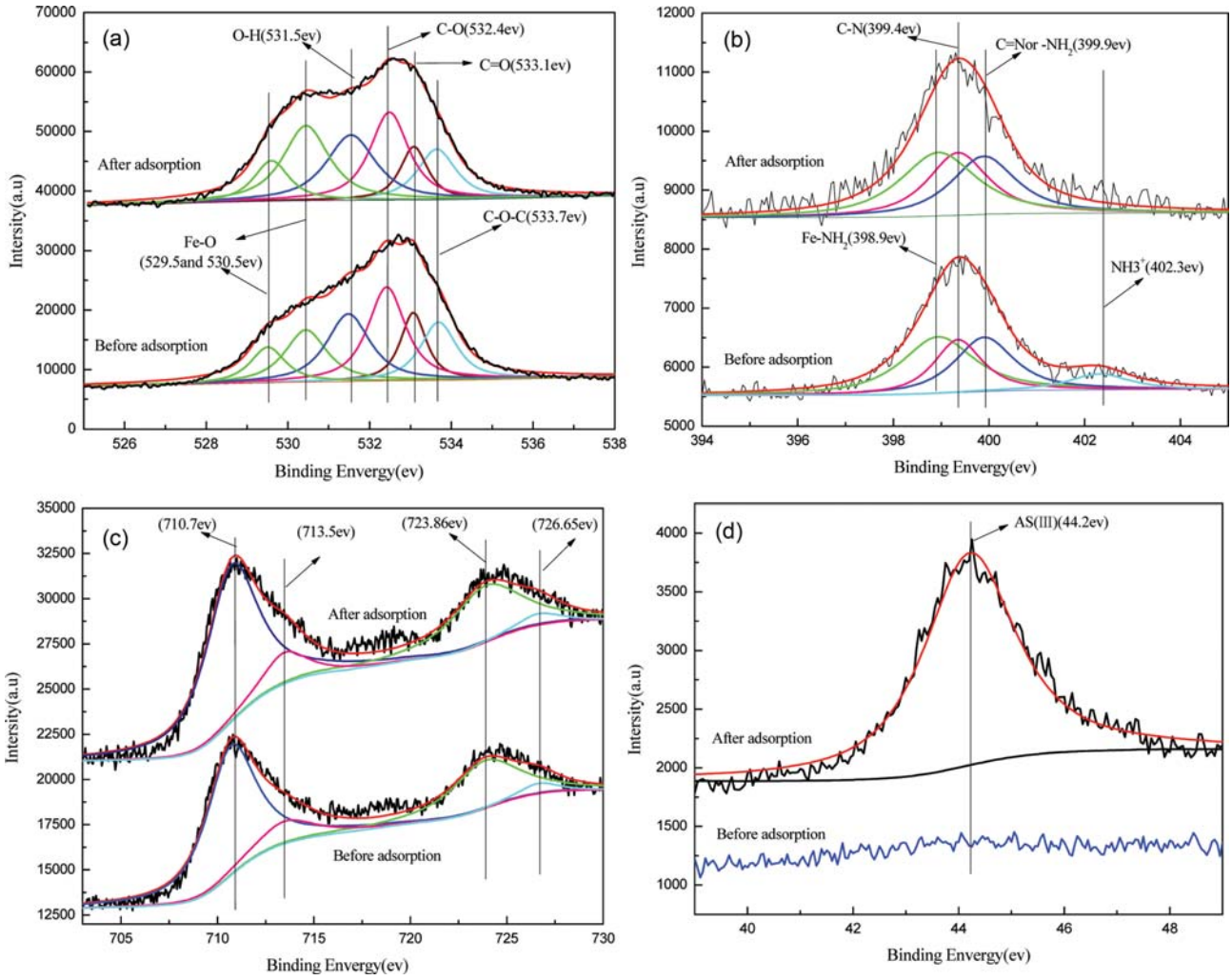

Fig. 12. XPS spectra of Fe-doped chitosan microsphere before and after adsorption of As(III) (a) O1s, (b) N1s, (c) Fe2p, (d) As3d.

resented C=N or -NH_2, C-N and the-NH_2 interacted with Fe(III), respectively [67,68]. The other peak at 402.3 eV was assigned to -NH_3^+ [68]. After adsorption, it was clearly demonstrated that the amount of -NH_3^+ functionalities was greatly reduced and disappeared after adsorption. Which was attributed to the fact that -NH_3^+ on chitosan was deprotonated to amino group during adsorption. As shown in Eq. (12), the equilibrium of reaction was shifted toward deprotonation in alkaline conditions [22,69]. Fig. 12(c) illustrates the XPS spectra of Fe2 p. The spectra of iron show peaks at 710.7 eV, 713.5 eV, 723.86 eV and 726.65 eV. The binding energy of the Fe 2 p was in good agreement with $Fe^{3+}2p_{3/2}$ and $Fe^{3+}2p_{1/2}$, respectively. The result indicates that the chemical valence of iron had no change during the adsorption process [70]. It was reported that the binding energies of the different chemical states of As 3d core levels for As(III) and As(V) were 44.1-44.5 eV and 45.2-45.6 eV, respectively [33,47]. As seen in Fig. 12(d), As 3d peak is presented. With the before adsorption comparatively speaking, there was an obvious peak at 44.2 eV after adsorption. The attachment of As ions onto iron-doped chitosan microsphere was suggested by the appearance of peak of As3d at 44.2 eV after adsorption. And the peak at 44.2 eV was assigned to As(III) [33,71]. Therefore, oxidation of As(III) could also be excluded in As(III)-iron-doped chitosan microsphere system.

$$\text{Chitosan-}NH_3^+ + H_2O \Leftrightarrow \text{Chitosan-}NH_2 + H_3O^+ \quad (12)$$

To further carry out the mechanism in the adsorption process, FT-IR analysis was conducted and the results are shown in Fig. 13. The peaks at 3,400, 2,867, 1,387 and 1,066 cm^{-1} indicate the stretching vibrations of O-H, C-H, -NH_2 and C-O-C bonds from chitosan, respectively [26,65,72]. After adsorption of arsenic, it is hypothesized that -NH_2 could act to form complexes with As(III). So the characteristic bands of -N-H at 1,387 cm^{-1} shifted to 1,371 cm^{-1}. The peak at 1,653 cm^{-1} could be attributed to C=N stretching vibrations or C=O stretching vibrations from amide band I [73-76]. The peak at 618 cm^{-1} was assigned to stretching vibration of Fe-O [4,32]. The disappeared peak at 1,564 cm^{-1} belongs to -NH_3^+ after adsorption. The result is consistent with Fig. 12(b). This further provided evidence that the -NH_3^+ on chitosan was deprotonated to amino group during adsorption (pH=8) [22]. The new peak at 819 cm^{-1} corresponds to Fe-O-As after adsorption [28,29,35,47]; the result is in accordance with Fig. 12(a). This indicates Fe plays a significant role in adsorption of As(III) on Iron-doped chitosan micro-

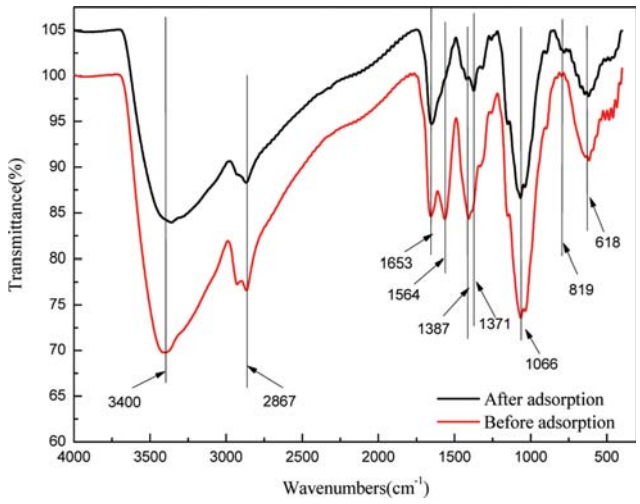

Fig. 13. FT-IR spectra of iron-doped chitosan microsphere before and after adsorption of As(III).

sphere. The arsenic adsorption could be responsible for a complexation between oxygen from As(III) (H_3AsO, H_2AsO^-, $HAsO_3^{2-}$ and AsO_3^{3-}) and the Fe through sharing their one lone pair of electrons. Iron-doped chitosan microsphere could adsorb As(III) by forming Fe-O-As coordination bonds.

CONCLUSIONS

An environmentally benign sorbent iron-doped chitosan microsphere was successfully prepared through a facile fabrication. Results showed that it was helpful for the adsorption of the As(III) onto iron-doped chitosan microsphere with the increase of iron content. The best adsorption performance was achieved at pH=8. For the adsorption kinetics, increase of the rotational speed was conducive to the adsorption rate, and the adsorption control process shifted from the liquid film diffusion to the chemical reaction process. Isotherm adsorption experiments showed that the adsorbent surface active sites were non-uniformly distributed and the adsorption was dominated by chemical adsorption. The adsorption process was spontaneous and exothermic. In presence of positive Pb^{2+}, Zn^{2+} and Cd^{2+} ions had negligible influence on the removal of As(III). However, the existence of anions (NO_3^-, SO_4^{2-} or PO_4^{3-}) inhibited the As(III) removal at different level. PO_4^{3-} showed the most significant side effects on the removal of As(III) by iron-doped chitosan microsphere. The regeneration of the saturated iron-doped chitosan microsphere could be performed using a simple treatment using 1.0 mol·L^{-1} NaOH. Upon recycling the adsorbent for three times only a meager 15.69% loss over its initial adsorption capacity was observed. XPS and FT-IR analysis showed that no valence change occurred before or after adsorption for iron and arsenic during the adsorption process. Adsorption of As(III) onto iron-chitosan microspheres was mainly achieved through the form of Fe-O-As.

ACKNOWLEDGEMENT

The authors are sincerely grateful to the Nature Science Foundation of Hubei Province for the financial grant for this research (project number 2015CFB550). Additional appreciation is given to the College of Resource and Environmental Science, South-Central University for Nationalities for chemical and apparatus support.

REFERENCES

1. A. F. D. de Namor, N. A. Hakawati, W. A. Hamdan, R. Soualhi, S. Korfali and L. Valiente, *J. Hazard. Mater.*, **326**, 61 (2017).
2. S. Aredes, B. Klein and M. Pawlik, *J. Clean Prod.*, **60**, 71 (2013).
3. W. S. Tang, Q. Li, S. Gao and J. K. Shang, *J. Hazard. Mater.*, **192**, 131 (2011).
4. S. O. Adio, M. H. Omar, M. Asif and T. A. Saleh, *Process Saf. Environ. Prot.*, **107**, 518 (2017).
5. D. Sribudda, T. Wannachod, P. Ramakul, U. Pancharoen and S. Phatanasri, *Korean J. Chem. Eng.*, **33**, 197 (2016).
6. Y. M. Hsueh, C. T. Su, H. S. Shiue, W. J. Chen, Y. S. Pu, Y. C. Lin, C. S. Tsai and C. Y. Huang, *Food Chem. Toxicol.*, **107**, 167 (2017).
7. A. Sattar, S. Y. Xie, M. A. Hafeez, X. Wang, H. I. Hussain, Z. Iqbal, Y. H. Pan, M. Iqbal, M. A. Shabbir and Z. H. Yuan, *Environ. Toxicol. Pharmacol.*, **48**, 214 (2016).
8. B. G. Wei, J. P. Yu, J. Wang, L. S. Yang, H. R. Li, C. Kong, Y. J. Xia and K. G. Wu, *Environ. Toxicol. Pharmacol.*, **53**, 89 (2017).
9. R. L. Hsieh, C. T. Su, H. S. Shiue, W. J. Chen, S. R. Huang, Y. C. Lin, M. I. Lin, S. C. Mu, R. J. Chen and Y. M. Hsueh, *Toxicol. Appl. Pharmacol.*, **321**, 37 (2017).
10. T. Roh, C. F. Lynch, P. Weyer, K. Wang, K. M. Kelly and G. Ludewig, *Environ. Res.*, **159**, 338 (2017).
11. A. M. Bandpei, S. M. Mohseni, A. Sheikhmohammadi, M. Sardar, M. Sarkhosh, M. Almasian, M. Avazpour, Z. Mosallanejad, Z. Atafar, S. Nazari and S. Rezaei, *Korean J. Chem. Eng.*, **34**, 376 (2017).
12. S. Chatterjee and S. De, *Sep. Purif. Technol.*, **179**, 357 (2017).
13. J. Kim, S. Han and Y. Kim, *Korean J. Chem. Eng.*, **34**, 2096 (2017).
14. Z. Oláh, T. Kremmer, A. T. Vogg, Z. Varga, Z. Szűcs, B. Neumaier and R. Dóczi, *Appl. Radiat. Isot.*, **122**, 111 (2017).
15. A. Ortega, I. Oliva, K. E. Contreras, I. González, M. R. Cruz-Díaz and E. P. Rivero, *Sep. Purif. Technol.*, **184**, 319 (2017).
16. B. F. Urbano, B. L. Rivas, F. Martinez and S. D. Alexandratos, *React. Funct. Polym.*, **72**, 642 (2012).
17. P. P. Song, Z. H. Yang, G. M. Zeng, X. Yang, H. Y. Xu, L. K. Wang, R. Xu, W. P. Xiong and K. Ahmad, *Chem. Eng. J.*, **317**, 707 (2017).
18. M. Sen, A. Manna and P. Pal, *J. Membr. Sci.*, **354**, 108 (2010).
19. Y. R. He, Y. P. Tang, D. C. Ma and T. S. Chung, *J. Membr. Sci.*, **541**, 262 (2017).
20. J. W. Ji, Y. B. Yun, Z. Zeng, R. C. Wang, X. Y. Zheng, L. H. Deng and C. L. Li, *Appl. Surf. Sci.*, **351**, 715 (2015).
21. D. W. Cho, B. H. Jeon, C. M. Chon, F. W. Schwartz, Y. Jeong and H. Song, *J. Ind. Eng. Chem.*, **28**, 60 (2015).
22. H. Liu, Z. J. Wei, M. Hu, Y. H. Deng, Z. Tong and C. Y. Wang, *RSC Adv.*, **4**, 29344 (2014).
23. S. Kumari, S. H. K. Annamareddy, S. Abanti and P. K. Rath, *Int. J. Biol. Macromol.*, **104**, 1697 (2017).
24. Y. G. Abou El-Reash, M. Otto, I. M. Kenawy and A. M. Ouf, *Int. J. Biol. Macromol.*, **49**, 513 (2011).
25. J. He, F. Bardelli, A. Gehin, E. Silvester and L. Charlet, *Water Res.*, **101**, 1 (2016).

26. H. B. Li, S. D. Bi, L. Liu, W. F. Dong and X. Wang, *Desalination*, **278**, 397 (2011).
27. N. M. Mahmoodi, B. Hayati, M. Arami and C. Lan, *Desalination*, **268**, 117 (2011).
28. Z. M. Liu, J. T. Chen, Y. C. Wu, Y. R. Li, J. Y. Zhao and P. Na, *J. Hazard. Mater.*, **343**, 304 (2018).
29. Z. H. Cheng, F. L. Fu, D. D. Dionysiou and B. Tang, *Water Res.*, **96**, 22 (2016).
30. S. I. Siddiqui and S. A. Chaudhry, *Process Saf. Environ. Prot.*, **111**, 592 (2017).
31. A. Kumar, J. Pandey and S. Kumar, *Korean J. Chem. Eng.*, **35**, 456 (2018).
32. D. D. Fu, Z. Q. He, S. S. Su, B. Xu, Y. L. Liu and Y. P. Zhao, *J. Colloid Interface Sci.*, **505**, 105 (2017).
33. Z. P. Wen, Y. L. Zhang, X. F. Zhou and R. Chen, *Sep. Purif. Technol.*, **176**, 395 (2017).
34. B. Tanhaei, A. Ayati, M. Lahtinen and M. Sillanpää, *Chem. Eng. J.*, **259**, 1 (2015).
35. K. Wu, R. P. Liu, T. Li, H. J. Liu, J. M. Peng and J. H. Qu, *Chem. Eng. J.*, **226**, 393 (2013).
36. W. Lazinski, W. Rudzinski and A. Plazinska, *Adv. Colloid Interface Sci.*, **152**, 2 (2009).
37. S. S. Gupta and K. G. Bhattacharyya, *Adv. Colloid Interface Sci.*, **162**, 39 (2011).
38. K. L. Tan and B. H. Hameed, *J. Taiwan Inst. Chem. Eng.*, **74**, 25 (2017).
39. J. P. Simonin, *Chem. Eng. J.*, **300**, 254 (2016).
40. H. M. Yu, J. Pang, T. Ai and L. Liu, *J. Taiwan Inst. Chem. Eng.*, **62**, 21 (2016).
41. F. T. Wang, Y. F. Pan, P. X. Cai, T. X. Guo and H. N. Xiao, *Bioresour. Technol.*, **241**, 482 (2017).
42. T. S. Singh and K. K. Pant, *Sep. Purif. Technol.*, **36**, 139 (2004).
43. J. M. Zhang, Z. H. Xiong, C. Li and C. S. Wu, *J. Mol. Liq.*, **221**, 43 (2016).
44. Y. Y. Xiong, J. Q. Li, L. L. Gong, X. F. Feng, L. N. Meng, L. Zhang, P. P. Meng, M. B. Luo and F. Luo, *J. Solid State Chem.*, **246**, 16 (2017).
45. M. D. G. de Luna, E. D. Flores, D. A. D. Genuino, C. M. Futalan and M. W. Wan, J. *Taiwan Inst. Chem. Eng.*, **44**, 646 (2013).
46. B. Kayranli, *Chem. Eng. J.*, **173**, 782 (2011).
47. Z. P. Wen, Y. L. Zhang, S. Guo and R. Chen, *J. Colloid Interface Sci.*, **486**, 211 (2017).
48. A. Teimouri, H. Esmaeili, R. Foroutan and B. Ramavandi, *Korean J. Chem. Eng.*, **35**, 479 (2017).
49. A. M. Nasir, P. S. Goh and A. F. Ismail, *Chemosphere*, **200**, 504 (2018).
50. S. Dawood and T. K. Sen, *Water Res.*, **46**, 1933 (2012).
51. M. S. Lashkenari, B. Davodi and H. Eisazadeh, *Korean J. Chem. Eng.*, **28**, 1532 (2011).
52. T. S. van Erp and J. A. Martens, *Micropor. Mesopor. Mater.*, **145**, 188 (2011).
53. N. Joshi, M. N. Romanias, V. Riffault and F. Thevenet, *Aeolian Res.*, **27**, 35 (2017).
54. A. K. Ladavos, A. P. Katsoulidis, A. Iosifidis, K. S. Triantafyllidis, T. J. Pinnavaia and P. J. Pomonis, *Micropor. Mesopor. Mater.*, **151**, 126 (2012).
55. J. Kim, C. Lee, S. M. Lee, Lalhmunsiama and J. Jung, *Ecotox. Environ. Safe.*, **147**, 80 (2018).
56. B. Chen, Z. L. Zhu, J. Ma, Y. L. Qiu and J. H. Chen, *J. Mater. Chem. A*, **1**, 11355 (2013).
57. J. Y. Qi, G. S. Zhang and H. N. Li, *Bioresour. Technol.*, **193**, 243 (2015).
58. L. N. Lin, W. W. Qiu, D. Wang, Q. Huang, Z. G. Song and H. W. Chau, *Ecotox. Environ. Safe.*, **144**, 514 (2017).
59. Z. P. Wen, Y. L. Zhang, Y. Wang, L. N. Li and R. Chen, *Chem. Eng. J.*, **312**, 39 (2017).
60. C. Liu, R. N. Jin, X. K. Ouyang and Y. G. Wang, *Appl. Surf. Sci.*, **408**, 77 (2017).
61. M. E. Argun, S. Dursun, C. Ozdemir and M. Karatas, *J. Hazard. Mater.*, **141**, 77 (2007).
62. Q. Y. Xie, Y. Li, Z. L. Lv, H. Zhou, X. J. Yang, J. Chen and H. Guo, *Sci. Rep.*, **7**, 3316 (2017).
63. G. R. Cui, M. Liu, Y. Chen, W. Zhang and J. Q. Zhao, *Carbohydr. Polym.*, **154**, 40 (2016).
64. J. Wang, W. H. Xu, L. Chen, X. J. Huang and J. H. Liu, *Chem. Eng. J.*, **251**, 25 (2014).
65. W. Wei, *Design of ionic barrier-based capsules and their application for selective recovery of precious metals*, Chonbuk National University, Republic of Korea (2016).
66. Y. W. Fen, W. M. M. Yunus and Z. A. Talib, *Optik*, **124**, 126 (2013).
67. S. W. Won, J. Park, J. Mao and Y. S. Yun, *Bioresour. Technol.*, **102**, 3888 (2011).
68. C. S. Shen, H. Chen, S. S. Wu, Y. Z. Wen, L. N. Li, Z. Jiang, M. C. Li and W. P. Liu, *J. Hazard. Mater.*, **244-245**, 689 (2013).
69. J. H. Jang, Y. M. Choi, Y. Y. Choi, M. K. Joo, M. H. Park, B. G. Choi, E. Y. Kang and B. Jeong, *J. Mater. Chem.*, **21**, 5484 (2011).
70. L. J. Song, Q. L. You, J. Li, Q. R. Cheng, G. Y. Liao, H. Xia and D. S. Wang, *Mater. Lett.*, **185**, 286 (2016).
71. B. B. Shao, Y. Y. Guan, Z. Y. Tian, X. H. Guan and D. L. Wu, *Colloids Surf., A.*, **506**, 703 (2016).
72. C. Valenzuela, V. Hernández, M. S. Morales, A. Neira-Carrillo and F. Pizarro, *LWT - Food Sci. Technol.*, **59**, 1283 (2014).
73. S. W. Won, I. S. Kwak and Y. S. Yun, *Bioresour. Technol.*, **160**, 93 (2014).
74. P. Bösiger, G. Tegl, I. M. T. Richard, L. L. Gat, L. Huber, V. Stagl, A. Mensah, G. M. Guebitz, R. M. Rossi and G. Fortunato, *Carbohydr. Polym.*, **181**, 551 (2018).
75. Y. Wang, E. L. Wang, Z. M. Wu, H. Li, Z. Zhu, X. S. Zhu and Y. Dong, *Carbohydr. Polym.*, **101**, 517 (2014).
76. Z. Cui, Y. Xiang, J. J. Si, M. Yang, Q. Zhang and T. Zhang, *Carbohydr. Polym.*, **73**, 111 (2008).